Curve-Fitting of MMC Transfer Functions to Assess Harmonic Stability

1st Lothar Brixius

[redacted]

[redacted]

***Abstract*—Global warming calls for an accelerated grid integration of renewable energy sources, which is done with the help of converters. The most common converter type used are modular multilevel converters (MMC). Converters can cause problems if they interact with the grid impedance, a phenomenon called harmonic instability. To prevent this, an analysis of the converter-grid connection is needed. In this paper, curve-fitting of an MMC transfer function (TF) presented to be used by a transmission system operator (TSO) for investigating said connection. While the paper does not address the topic of modelling the grid impedance, it will explain the methods established in literature to make use of the fitted MMC TFs if a grid TF is provided. A common approach for stability assessment is the Nyquist Criterion. However, it will be shown that this is not ideal for the task at hand and instead the Bode plot should be investigated, as proposed in literature. The curve-fitting is based on virtual measurements of black-box converter models. A blanc function to be optimized is theoretically deduced. Lastly, one way to numerically perform the curve-fitting in MATLAB is presented. It is shown that the numerically derived transfer function with five poles and zero crossings best matches the analytical expression derived from literature.**

***Index Terms*—harmonic stability, harmonic instability, modular multilevel converter, MMC, transmission system operator, TSO**

I. Introduction

Due to global warming, the usage of emission-neutral energy sources has become increasingly important over the last couple of years, see Table 1 in [4]. Usually this is done with the help of converters. Modular Multilevel Converters (MMC) [5] are "becoming the worldwide standard for HVDC ", p.1 in [21], hence this paper focuses on curve-fitting transfer functions (TF) of MMCs. From the perspective of a Transmission System Operator (TSO) the integration of renewable energy sources means additional problems when ensuring grid stability. One example would be offshore windfarms, since maintenance and construction are hard to realize kilometres away from the mainland. Investigation of faults is key for keeping the costs minimal [13] [14]. Multiple forced shutdowns of such windfarms have been reported in the past [1]. The reason for those shut-downs was harmonic instability, which is caused by interactions between converter and grid impedance. The impedance of a converter depends on its operating points, for example influenced by its controls [2]. Since converters change operating points at a fast pace, a detailed look into the controls is required [14]. Another source of these problems is a change in the frequency dependent impedance of the grid [1], which will not be addressed in this paper. However, from the point of a TSO the controls of a converter, and thus its impedance $\underline{Z}_c$ as a function of the controller switching frequency s_c is unknown. The reason for this is that device manufacturers do not provide this information to protect themselves from reverse engineering. So instead, TSOs need to perform virtual measurements with provided black-box models or laboratory experiments to investigate $\underline{Z}_c(s_c)$; this paper sets out to be a guideline for performing this task.

The rest of the paper is structured as follows: Section 2 provides an introduction into harmonic stability and theoretical analysis of the converter-grid connection and methods for stability assessment. It is explained why an investigation of the Bode plot should be used instead of the Nyquist criterion. Section 3 presents a theoretical deduction of a generic transfer function (TF) of an MMC operated with a closed-loop control scheme based on literature [3] showing that the most promising function for curve fitting will have five poles and four zero crossings. Section 4 describes the setup for the virtual measurement of MMC impedance, as presented in [2] used to generate measurement data for the curve fitting. Section 5 then explains how to process the generated data and perform a numerical determination of the TF's coefficients. As a last step, Section 6 discusses the quality of the calculated TFs. It is shown that the numerically derived transfer function with five poles and zero crossings best matches the analytical expression derived from literature.

II. Stability Assessment

A. Harmonic Stability

The problem tackled in this paper is called harmonic instability. The following definition can be found on p.100 [3]: "Harmonic instability is the condition in which a natural frequency of the network is excited because a given or several installations are adversely controlling the energy in the system, leading to oscillations with non-decreasing amplitude at that frequency [...]". The surplus of energy flowing into the circuit is transferred as an oscillation of the energy stored

between the electric and magnetic fields. A natural frequency is the frequency of a wave component present in a network voltage or current oscillation after the network is subjected to a disturbance, excluding the frequencies of components in the exciting signals." Harmonic instability can be the result of an interaction between the electromagnetic properties of the network and the dynamics of a converter, which may be affected by resonances [3].

Consequently, harmonic stability describes the condition where those events do not emerge. Harmonic instability can be observed as oscillations in the grid; it can lead to a forced shutdown of components or a network failure. Aside from these voltage disturbances, current spikes occur, high enough to damage grid devices. To ensure harmonic stability, an analysis of the converter-grid connection is needed. This is especially important since the number of power electronic devices in the grid will rise as more and more renewable energy sources are installed. Additionally, the shutdown of large, conventional power plants, e.g., coal-fired ones, leads to a loss in system inertia and thereby a lesser damping of frequency oscillations p.1 in [6].

B. Modelling the Converter-Grid Connection

To simplify modelling the converter-grid interactions, one wants to reduce the three-phase AC reality into a single-phase equivalent circuit diagram (ECD). As a first step, the device elements are considered in frequency domain. A reduction to a single phase is possible if a symmetrical load is established, p.308 in [15]. This means a) that coupling impedances between the converter legs must be negligible or symmetrical and b) the distribution between activated and deactivated modules must be the same for each leg. The latter can be understood by looking at Fig. 1 and assuming a grid impedance approaching zero, which would result in a parallel connection of both arms for each phase. The parallel impedance of phase i will

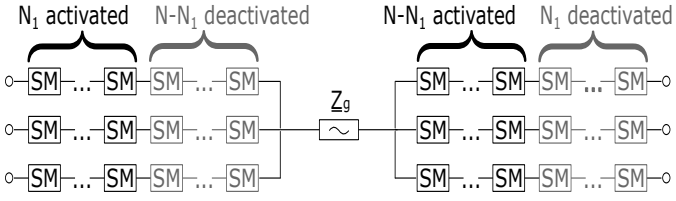

Fig. 1. "Unfolding" the lower and upper leg of an MMC. N denotes the number of total SMs to achieve the desired DC voltage. N_1 exemplarily the number of activated SMs on the upper leg for one phase.

then be determined by the ratio $\frac{(N-N_i)*N_i}{N-N_i+N_i}$, leading to the requirement of $N_1 = N_2 = N_3$. N_i denotes the number of activated submodules (SM) for phase i and N the number of total SMs to achieve the desired DC voltage. The fulfilment of this condition will depend on the chosen control method, see section 3 in [22]. In case no symmetrical load can be provided, decoupling can still be done via positive, negative and zero sequence vectors, see chapter 8.11 in [16], note that this does not require a symmetrical load. Similarly, Clarke's $\alpha\beta 0$ transformation or Park's $dq0$ transformation can be used. From here on, the $dq0$ transformation will be applied. A detailed description can be found in chapter 8.11.4 in [16]. Most of the time, the 0-component can be eliminated, p.112 [3]. Then, the impedance of the converter can be calculated with d and q component only according to eq. 9-13 [3] with the following equation:

$$\frac{\underline{U}_{c,dq}}{\underline{U}_{g,dq}} = \frac{1}{1 + \underline{Z}_{g,dq}\underline{Y}_{c,dq}} \tag{1}$$

which corresponds to the following ECD: Notice that a neglection of the 0 component implies a balanced three-phase system, meaning as soon as a fault appears this might no longer be valid. Also keep in mind that for positive, negative and zero sequence vectors, three different ESDs must be considered, see fig. 8.39 on p. 269 in [16]. This means $\underline{Z}_c$ must be modelled differently three times. The same will in general be true for $dq0$ transform, even with the 0 component being negligible, see fig. 8.46 on p.283 [16] where this is demonstrated for a synchronous machine.

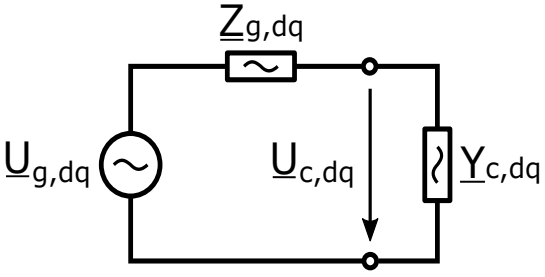

Fig. 2. Equivalent circuit diagram after the dq-transform. Similar concept for a single-phase ECD in case of a symmetrical load. Taken from p.112 [1]. $\underline{U}_g$, $\underline{Z}_g$ denote grid voltage and impeance and $\underline{U}_c$, $\underline{Y}_c$ the converter voltage and admittance. Everything is considered in the dq domain.

C. Applying the Nyquist Criterion

The Nyquist Criterion (NC) is one of the most common tools in analysing the stability of systems. A description and mathematical deduction can be found in literature, see for example chapter 4.4 in [7]. It is frequently used for assessing the stability of closed loop systems and can be applied for time-continuous and -discrete systems. If the closed loop system is described by:

$$\frac{G(s)}{1 + G(s)H(s)} \tag{2}$$

then the plot of the open loop frequency response $G(s)H(s)$ is required. Since $\underline{Y}_c(s) = \frac{1}{\underline{Z}_c(s)}$ and $\underline{Z}_g(s)$ are "inherently stable", p.109 [1], the NC can be applied to Eq. 1 by identifying the TF of the open loop system as $G(s)H(s)$. It is assumed that the TSO has knowledge of $\underline{Z}_g(s)$ at the converter-grid connection point. Measuring the converter impedance for various points will then allow the creation of the Nyquist plot. However, this approach does not allow an analytical assessment of the poles and zero-crossings. Furthermore, it only provides an abstract quantitative indication of stability in terms of phase and gain margin. Additionally, a Nyquist plot should depict a range of $0 \leq \omega \leq \infty$.

D. Alternative: Bode-Plot

Because of the drawbacks of the NC discussed above, it is rather suggested to use the Bode-plot for stability assessment as suggested in [3], p.110. Looking back at Eq. 1 the transfer function becomes infinity, meaning the system becomes unstable, when $\underline{Z}_g(s) + \underline{Z}_c(s) = 0$. For complex numbers, this means similar amplitude and phases shifted by around $180°$. This consideration allows for an intuitive quantitative description of converter-grid stability via the following definitions:

$$Z_{diff}(s) := \left| |\underline{Z}_g(s)| - |\underline{Z}_c(s)| \right| \tag{3}$$

$$\varphi_{diff}(s) := \varphi_g(s) - \varphi_c(s) \tag{4}$$

which will be called magnitude and phase difference respectively. Harmonic instability will occur if

$$Z_{diff} \approx 0\,\Omega \ \wedge \ \varphi \approx \pm 180° \tag{5}$$

Analysing incidences of the past, TSOs or public institutions can use Z_{diff} and φ_{diff} to define safety margins. Unlike the phase and gain margin from the Nyquist criterion, they can be directly linked to the current in case of a disturbance. Another advantage of the bode plot is, that it has only to be analysed for the frequency range where harmonic stability problems can occur. This range goes from $100\ Hz$ up to several kHz, p.99 in [3]. No matter if the NC or the Bode Plot is used for assessing stability of the converter-grid connection, one still may want to know the exact position of the TF's poles. To achieve this, curve-fitting could be used to determine numerical values for the coefficient of a prototype function. The question is: How does this prototype function look like?

III. Transfer Function Derivation

Since TSOs will not be provided with a detailed model by the converter's manufacturer, one must analyse a generic model, or look for references in literature. Here, we want to use the deduction in [18] for an MMC operated with a closed-loop control scheme. Equation 15 in Appendix B states the result for the converter admittance. For a derivation, please also look at the appendix. It can be seen that the resulting TF has four zero crossings and four poles. However, this is only valid for closed-loop systems. Open loop TFs are more complex [18]. It might even be impossible to get a limited range of possible orders for the TFs, since they heavily depend on the control scheme used [18] [19].

IV. Taking Virtual Measurements

For taking virtual measurements, we have used the setup proposed in [2] of an MMC Model. In an industry context, this would be a black-box model provided by the manufacturer to the TSO. Taking measurements of a real converter comes with less flexibility but ensures an accurate response. One possible way to set this up can be found in section IV in [18]. The virtual measurements were performed with the help of an MMC model implemented in MATLAB/Simulink™. For a discussion of how the model works and how it is set up, please refer to [2], especially section 3. Here, only the impedance measurement method will be briefly recapped:
An operating point for the converter is set and a small perturbation voltage applied. After some time, the transient processes have declined, and the measurement is performed. Small signal in this case means an amplitude of 5 to 20 % in comparison to the grid voltage. The voltage and current need to be recorded at the point of measurement, e.g., the AC terminal of the MMC. Then a Fourier analysis must be performed to detect the components with the same frequency as the small signal voltage source and by applying Ohm's Law to these components, the resulting impedance can be calculated. The frequency of the small signal needs to be varied (and tracked) to achieve a set of data points. The entire simulation consists of two MMCs, connecting two grids via a DC line. The controls of the MMC consists of multiple PI control levels and is modelled according to [11]. Fig. 3 shows the overall principle of the impedance measurement method. For more details, please refer to [2].

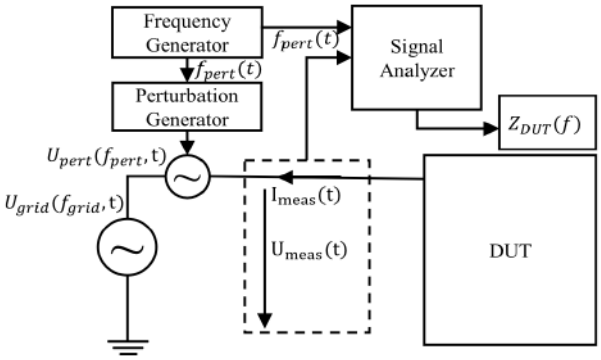

Fig. 3. Impedance measurement method overview. Taken from [2]

V. Processing Measurement Data

A. Interpolation

There exist various means to interpolate between the measurement points. To use non-complex methods, either real- and imaginary part can be considered separately or amplitude and phase. One possibility would be Lagrange- or Chebyshev polynomials [8], or Spline interpolation, see chapter 8 in [9]. Their properties, for example calculation time and numerical accuracy, have been thoroughly investigated in mathematical literature. This method is disregarded here because it does not result in a closed expression for the TF and hence does not allow for an analysis of poles and zero-crossings.

B. Curve Fitting

In this paper we want to focus on a method for determining the coefficients of the complex broken rational polynomial in Eq. 15 deduced in Appendix B. With the fundamental sentence of algebra [10] the following identity holds true, allowing for an analysis of poles and zero-crossings. In the notation of p.106 in [1]:

$$Y_c(s_c) = \frac{\sum_{i=0}^{n} a_i s_c^i}{\sum_{i=0}^{m} b_i s_c^i} = K \frac{\prod_{i=1}^{n} (s_c + c_i)}{\prod_{i=1}^{n} (s_c + d_i)} \tag{6}$$

The coefficients of Eq. 6 need to be optimized with the help of the data set. For this, methods such as Maximum-Likelihood [20]or Non-Linear Least Squares Algorithm [12] can be used. Maximum-Likelihood works by finding a function that fits best to the distributions provided (e.g. the data points). Various implementations of these algorithms can be found as closed or open software. Here the System Identification Toolbox™ (SIT) of MATLAB™ was chosen as the MMC model was also implemented in MATLAB™. The option-box "enforce stability" was checked assuming the MMC on its own is stable, p.109 [1]. The following table presents the most important parameters of the MMC simulation. For details, please refer to [2]. K_p and K_i to the proportional and integral part of the AC-Side-Current-Controller (ACCC).

TABLE I
MMC PARAMETERS

Parameter	***Value***
Transferred Power	$1.3\ kW$
Connected grid-voltage RMS	$204\ V$
Transmission Line Voltage DC	$650\ V$
Arm Inductance	$50\ mH$
K_p ACCC	1
K_i ACCC	100

VI. RESULTS

In this section, the following description is used for TFs: x/y, denotes the number of zero crossings and y number of poles. For MATLAB™ to perform calculations correctly, it turned out to be necessary to have a higher number of poles than zero-crossings, meaning $m > n$ in Eq. 6. The numerical results can be found in Appendix A. For purposes of validation, The optimization was also applied to a 1/2 and 9/10 TF. Both time-continuous and time-discrete functions were investigated. The sampling time for the time-discrete case was set to $50\ \mu s$. To determine their quality, the relative error e was calculated according to:

$$e(TF) := \frac{1}{n}\sum_{i=1}^{n}\frac{TF(f_i) - m(f_i)}{m(f_i)} \tag{7}$$

Where n is the number of measurement points, f_i the frequency at which the measurement was performed and $TF(f_i)$ the evaluation of a TF at f_i. One can see that the errors are

TABLE II
TRANSFER FUNCTION ACCURACY

x/y	***Time Continuous***	***Time Discrete***
1/2	93 %	99 %
4/5	25 %	108 %
4/5 (stability not enforced)	5 %	-
9/10	194 %	116 %

high. It can also be seen that the function aligning with the analytically deduced number of poles and zero-crossings gives the best result. Lifting the "enforced stability" requirement allowed for a smaller error of 5 %. The reason for this and the missing reduction of $e(TF)$ for the 4/5 discrete case are unknown to the authors. It is worth noting that every determined TF had margin stable poles, as can be seen in the figures below. For the 4/5 TF without enforced stability, SIT™ returned unstable poles.

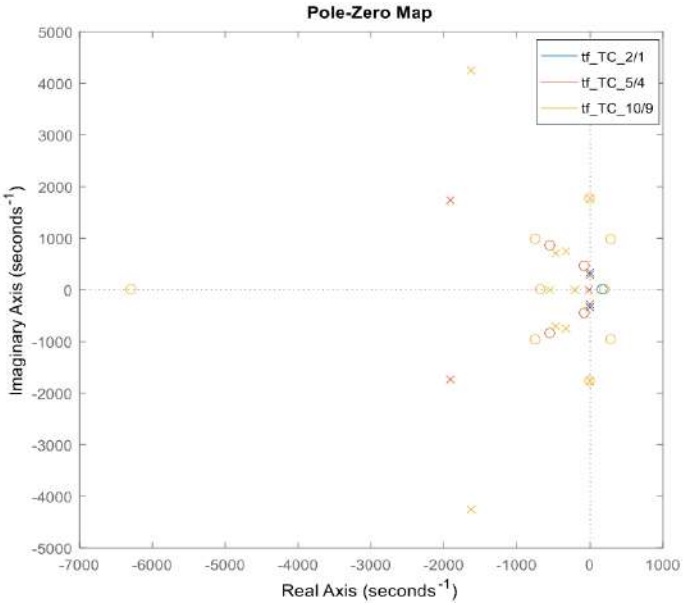

Fig. 4. Location of the poles and zero crossings of the determined time continuous TFs in the s plane.

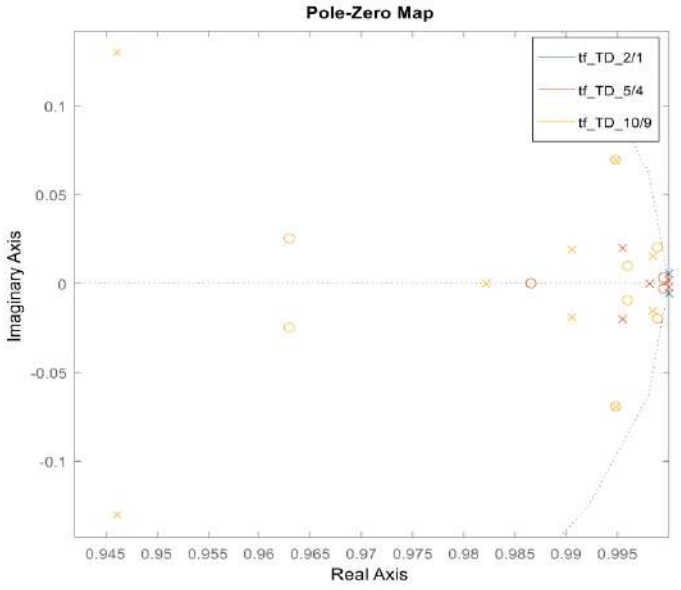

Fig. 5. Location of the poles and zero crossings of the determined time continuous TFs in the z plane.

VII. CONCLUSION

This paper presents a method to investigate harmonic stability for converter-grid connections from the perspective of a TSO. Working with virtual measurement data, a TSO still can

perform a stability analysis using curve-fitting or interpolation. The resulting TFs can, but should not, be used in combination with the Nyquist criterion. Rather, it seems recommendable to investigate the Bode plot. It was shown how a theoretical investigation of converter topology and controls can be used to receive prototype functions, whose coefficients can be numerically determined with help of the measurement set. Depending on the chosen control, the amount of poles and zero crossings will be around five each.

ACKNOWLEDGMENT

This paper is based on the bachelor thesis written by Lothar Brixius at the former chair for high voltage electronics IFHT of the RWTH Aachen University, nowadays part of IAEW. He wants to wholeheartedly thank his two supervisors, Matthias Quester and Viswaja Yellisetti.

REFERENCES

[1] N. Shore, Y. Fillion, K. Hermanns et al., "AC side harmonics and appropriate harmonic limits for VSC HVDC," CIGRE technical brochure 754, ISBN : 978-2-85873-456-6, February 2019.

[2] M. Quester, F. Loku, V. Yellisetti and R. Puffer, "Online Impedance Measurement of a Modular Multilevel Converter," DOI: 10.1109/ISGTEurope.2019.8905769, 2019

[3] L. Bessegato, "A Method for the Calculation of the AC-Side Admittance of a Modular Multilevel Converter," IEEE TRANSACTIONS ON POWER ELECTRONICS, VOL. 34, NO. 5 2019, 2018

[4] A. Q. Al-Shetwi, "Sustainable development of renewable energy integrated power sector: Trends, environmental impacts, and recent challenges," Science of the Total Environment 822 (2022) 153645, http://dx.doi.org/10.1016/j.scitotenv.2022.153645, February 2022

[5] R. Marquardt, "Modular Multilevel Converters – State of the Art and Future Progress," IEEE Power Electronics Magazine, DOI 10.1109/MPEL.2018.2873496, December 2018

[6] M. Schönefeld, J. Hüllenkremer, M. Siemonsmeier, A. Moser, O. Anaya-Lara and D. Campos-Gaona, "Frequency stability analysis under consideration of virtual inertia emulation of converter-interfaced hydropower plants in the Nordic Transmission Grid," 3rd SEERC Conference 2020, 2020

[7] S. Palani, "Automatic Control Systems," Springer, https://doi.org/10.1007/978-3-030-93445-3_4, 2022

[8] J.-P. Berrut and L. Trefethen, "Barycentric Lagrange Interpolation," SIAM Review Vol. 46, No. 3, pp. 501-517, DOI. 10.1137/S0036144502417715, 2004

[9] P. Turner, "Numerical Analysis," The Macmillan Press LTD, ISBN 978-0-333-58665-5, DOI 10.1007/978-1-349-13108-2, 1994

[10] B. Fine and G. Rosenberger, "The Fundamental Theorem of Algebra," Springer, ISBN 978-0-387-94657-3, https://doi.org/10.1007/978-1-4612-1928-6, 1997

[11] H. Saad, Y. Fillion, S. Deschanvres, Y. Vernay, and S. Dennetire, "On Resonances and Harmonics in HVDC-MMC Station Connected to AC Grid," IEEE Transactions on Power Delivery, vol. 32, no. 3, pp. 1565–1573, June 2017

[12] B. V. Elsevier, "Advanced Data Analysis and Modelling in Chemical Engineering," Chapter 9.1, http://dx.doi.org/10.1016/B978-0-444-59485-3.00009-6, 2017

[13] C.Buchhagen, "BorWin1 – First Experiences with Harmonic Interactions in Converter Dominated Grids," International ETG Congress 2015, VDE VERLAG GMBH – Ber- lin – Offenbach, 2015

[14] C. Buchhagen, "Harmonic Stability – Practical Experience of a TSO," 2015

[15] K. Friedrich Schäfer, "Netzberechnung," (Grid Calculations) Springer, ISBN 978-3-658-40876-3, 2022

[16] A. J. Schwab, "Elektroenergiesysteme," 6th Edition, Springer Nature, ISBN 978-3-662-60373-4, https://doi.org/10.1007/978-3-662-60374-1, 2020

[17] B. Wen, D. Boroyevich, R. Burgos, P. Mattavelli, and Z. Shen, "Analysis of D-Q Small-Signal Impedance of Grid-Tied Inverters," IEEE Transactions on Power Electronics, vol. 31, no. 1, pp. 675-687, January 2016

[18] L. Bessegato, K. Ileves, L. Harnefors, and S. Norrga "Effects of Control on the AC-Side Admittance of a Modular Multilevel Converter," IEEE TRANSACTIONS ON POWER ELECTRONICS, VOL. 34, NO. 8 2019, 2018

[19] L. Bessegato, "A Method for the Calculation of the AC-Side Admittance of a Modular Multilevel Converter," IEEE TRANSACTIONS ON POWER ELECTRONICS, VOL. 34, NO. 5 2019, 2018

[20] T. Brox, and K. Ikeuchi, "Computer Vision," Chapter, pp. 481-482, Springer, Boston, MA. DOI 10.1007/978-0-387-31439-6_674, 2014

[21] R. Marquardt, "Modular Multilevel Converters: State of the Art and Future Progress," in IEEE Power Electronics Magazine, vol. 5, no. 4, pp. 24-31, Dec. 2018, doi: 10.1109/MPEL.2018.2873496.

[22] G. S. Konstantinou and V. G. Agelidis, "Performance evaluation of half-bridge cascaded multilevel converters operated with multicarrier sinusoidal PWM techniques," 2009 4th IEEE Conference on Industrial Electronics and Applications, Xi'an, China, 2009, pp. 3399-3404, doi: 10.1109/ICIEA.2009.5138833.

APPENDIX

A. DETERMINED TRANSFER FUNCTIONS

Numerically determined coefficients for Z_{MMC} from MATLAB's System Identification Toolbox™. Units are not provided to improve readability. Coefficients are rounded to 1 or 2 significant numbers.

Time Continuous with Two Poles

$$\frac{-7508s + 1.32 \cdot 10^6}{s^2 + 0.004s + 1.13 \cdot 10^5} \tag{8}$$

Time Continuous with Five Poles

$$\frac{2.75 \cdot 10^5 s^4 + 3.36 \cdot 10^8 s^3 + 3.82 \cdot 10^{11} s^2 + 1.04 \cdot 10^{14} s + 6 \cdot 10^{16}}{s^5 + 3840 s^4 + 6.81 \cdot 10^6 s^3 + 4.07 \cdot 10^{11} s^2 + 5.37 \cdot 10^{11} s + 8.04 \cdot 10^{12}} \tag{9}$$

Time Continuous with Ten Poles

$$\frac{1.6 \cdot 10^5 s^9 + 1.2 \cdot 10^9 s^8 + 2.2 \cdot 10^{12} s^7 + 6 \cdot 10^{15} s^6 + 6.8 \cdot 10^{18} s^5 + 8.4 \cdot 10^{21} s^4 + 5.4 \cdot 10^{26} s^3 + 5.1 \cdot 10^{27} s^2 + 2 \cdot 10^{30} s - 6.7 \cdot 10^{32}}{s^{10} + 5600 s^9 + 3.5 \cdot 10^7 s^8 + 8 \cdot 10^{10} s^7 + 1.8 \cdot 10^{16} s^6 + 2.6 \cdot 10^{17} s^5 + 2.8 \cdot 10^{20} s^6 + 2 \cdot 10^{23} s^3 + 1 \cdot 10^{26} s^2 + 3.2 \cdot 10^{28} s - 3.5 \cdot 10^{30}} \tag{10}$$

Time Discrete with Two Poles

$$\frac{0.004 z^{-1}}{2z^{-1} + z^{-2} + 0.99} \tag{11}$$

Time Discrete with Five Poles

$$\frac{7.48 \cdot 10^{-3} z^{-1} + 22.34 \cdot 10^{-3} z^{-2} + 22.23 \cdot 10^{-3} z^{-3} + 7.38 \cdot 10^{-3} z^{-4}}{-4.99 z^{-1} + 9.957 z^{-2} + 9.936 + z^{-3} + 4.96 z^{-3} + 5.37 z^{-4} + 0.99} \tag{12}$$

Time Discrete with Ten Poles

$$\frac{1.46 z^{-1} - 11.55 z^{-2} + 39.96 z^{-3} - 79 z^{-4} + 97.64 z^{-5} - 77.25 z^{-6} + 38.2 z^{-7} + 10 z^{-8} + 1.34 z^{-9}}{9.73 z^{-1} + 42.6 z^{-2} + 110.6 z^{-3} + 188.5 z^{-4} - 220.4 z^{-5} + 179 z^{-6} + 99.76 z^{-7} + 36.49 z^{-8} + 7.914 z^{-9} + 0.773 z^{-10} + 0.99} \tag{13}$$

Time Continuous with Five Poles without Enforced Stability

$$\frac{1.03 \cdot 10^5 s^4 + 3.3 \cdot 10^9 s^3 + 3.62 \cdot 10^{11} s^2 + 1.15 \cdot 10^{14} s + 6.37 \cdot 10^{16}}{s^5 - 830.7 s^4 + 9.25 \cdot 10^6 s^3 - 5.73 \cdot 10^8 s^2 + 9.03 \cdot 10^{11} s - 1.3 \cdot 10^{13}} \tag{14}$$

B. Derivation of the MMC Transfer Function

Final result for the AC side admittance of an MMC, based on [18] [19].

$$Y_{ac}(s_p) = \frac{e_1^* s_{p1}^4 + a_3 s_{p1}^3 + a_2 s_{p1}^2 + a_1 s_{p1} + a_0}{e_1^* s_p s_{p1}^4 + b_{41} s_{p1}^4 + b_{42} s_p s_{p1}^3 + b_{31} s_{p1}^3 + b_{32} s_p s_{p1}^2 + b_{21} s_{p1}^2 + b_{22} s_p s_{p1} + b_{11} s_{p1} + b_0} \tag{15}$$

where $s_{p1} \coloneqq s_p - s_1$, $a_3 = a_{lpf} e_1^*$, $a_2 = 2c_2 - c_4 + 0.5c_5(s_1 - a_s)$, $a_1 = E(s_1) a_f a_{lpf} a_p - c_4 a_f + c_5(-a_s(a_1 + 0.5a_f) + 0.5 a_f s_1)$, $a_0 = c_5(-a_1 a_f a_s)$, $b_{41} = e_1^* c_1$, $b_{42} = 0.5 e_1^* a_{lpf} L$, $b_{31} = e_1^*(c_1(a_{lpf} + a_f) + L a_1 a_s)$, $b_{32} = 0.5L(c_2 + e_1^* a_f a_{lpf})$, $b_{21} = c_3(a_{lpf} + a_f) + c_1 c_2$, $b_{22} = c_2 L a_f a_1 a_s$, $b_{11} = c_2 L a_1 a_s + a_f(e_1^* a_{lpf} + c_1 c_2)$, $b_0 = c_2 L a_f a_s a_1$, $c_1 \coloneqq 0.5(R + L(a_s + s_1))$, $c_2 \coloneqq 2Re\{E(s_1)\} a_{lpf} a_p$, $c_3 \coloneqq e_1^* L a_1 a_s$, $c_4 \coloneqq V_s^* a_{lpf} a_p$, $c_5 \coloneqq I_1 L a_{lpf} a_p$ and $E(s_1)$ are the Fourier transforms of the voltage at perturbation frequency s_p and the PCC voltage, respectively. L and R denote the arm inductance and resistance. Every α corresponds to a controller parameter, see [18] [19]. $I_s(s_1)$ denotes the Fourier transform of the AC side current. e_1^* denotes the reference value for the PCC voltage amplitude.

The starting point for the derivation is Eq. 65 in [18]:

$$Y_{ac}(s_p) = \frac{1 + \big(H_{PLL} - H_{dq}(s_p - s_1)\big) e^{-s_p T_d}}{\frac{s_p L + R}{2} + \big(F_{dq}(s_p - s_1) - \frac{s_1 L}{2}\big) e^{-s_p T_d}} \tag{16}$$

"where H_{PLL} groups the effects of the PLL on the admittance, induced by the dq transform and its inverse", p.8, Eq. 66 [18]:

$$H_{PLL} = \left[\left(-F_{dq}(s_p - s_1) + \frac{s_1 L}{2} \right) I_s(s_1) + H_{dq}(s_p - s_1) E(s_1) - V_s^*(s_1) \right] \frac{j X_\varepsilon(s_p - s_1)}{E(s_p)} \tag{17}$$

F_{dq} is a proportional integral controller, Eq. 21 on p. 4 of [18]:

$$F_{dq}(s_p - s_1) = \alpha_s \frac{L}{2} \left(1 + \frac{2\alpha_1}{s_p - s_1} \right) \tag{18}$$

and H_{dq} a low-pass filter with bandwidth α_f, Eq. 22 on p.4 [18]:

$$H_{dq}(s_p - s_1) = \frac{\alpha_f}{s_p - s_1 + \alpha_f} \tag{19}$$

next, $X_\varepsilon(s_p - s_1)$ denotes the perturbation frequency component at the output of the PLL, Eq. 47 on p.7 [18]:

$$X_\varepsilon(s_p - s_1) = \frac{-j H_p(s_p - s_1)}{1 + 2Re\{E(s_1)\} H_p(s_p - s_1)} E(f_p) \tag{20}$$

with the PLL open-loop transfer function $H_p(s)$ given by Eq. 46 p.7 in [18] as:

$$H_p(s_p - s_1) = \frac{\alpha_p H_{lpf}(s_p - s_1)}{e_1^*(s_p - s_1)} \tag{21}$$

furthermore $E(s_1) = \frac{e_1}{2}$ and $E(s_p) = \frac{e_p}{2}$, p.7 [18], with e_p and e_1 being the amplitude of the time-domain PCC and perturbation voltage, Eq. 26 on p.5 [18]. Finally, $V_s^*(s_1)$ is the Fourier transform, according to Eq. 48 on p. 7 [18]:

$$V_s^*(s_1) = e_1^* \delta(s_1) \tag{22}$$

where $\delta(s)$ denotes the Dirac function. It is assumed that H_{lpf} representing a generic low pass filter of first order, since no details are provided in the mentioned paper.

$$H_{lpf}(s_p - s_1) = \frac{\alpha_{lpf}}{s_p - s_1 + \alpha_{lpf}},\ \alpha_{lpf} \in \mathbb{R} \tag{23}$$

Inserting each equation into Y_{ac} and simplifying said expression is done via Julia v1.9.3, JupyterNotebook v6.5.2 and Symbolics v5.10.0:

In [20]:

```
using Symbolics
@variables s_p, s_1, s_p1 L, R, I_1, Re_E1, E_p, E_1, e_1star, V_sstar, a_f, a_s, a_1, a_lpf, a_p
function F_dq(s_p1)
    a_s*L/2*(1+2*a_1/(s_p1))
end
function H_dq(s_p1)
    a_f/(s_p1+a_f)
end
function H_lpf(s_p1)
    a_lpf/(s_p1+a_lpf)
end
function H_p(s_p1)
    a_p*H_lpf(s_p1)/(e_1star*(s_p1))
end
function X_e(s_p1)
    -1im*H_p(s_p1)*E_p/(1+2*Re_E1*H_p(s_p1))
end
function H_PLL(s_p)
    ((-F_dq(s_p1)+(s_1*L)/2)*I_1+H_dq(s_p1)*E_1-V_sstar)*(1im*X_e(s_p1))/E_p
end
simplify((1+H_PLL(s_p1)-H_dq(s_p1))/((s_p*L+R)/(2) +(F_dq(s_p1)-(s_1*L)/2) ))
```

Out[20]:

$$\frac{E_1 a_f a_{lpf} a_p s_{p1} + 2 s_{p1}^2 Re_{E1} a_{lpf} a_p - V_{sstar} a_f a_{lpf} a_p s_{p1} - s_{p1}^2 V_{sstar} a_{lpf} a_p + s_{p1}^3 a_{lpf} e_{1star} + s_{p1}^4 e_{1star} - I_1 La_1 a_f a_{lpf} a_p a_s - I_1 La_1 a_{lpf} a_p a_s s_{p1} - \frac{1}{2} I_1 La_f a_{lpf} a_p a_s s_{p1} + \frac{1}{2} I_1 La_f a_{lpf} a_p s_1 s_{p1} - \frac{1}{2} s_{p1}^2 I_1 La_{lpf} a_p a_s + \frac{1}{2} s_{p1}^2 I_1 La_{lpf} a_p s_1}{\left(\frac{1}{2} Rs_{p1} + La_1 a_s + \frac{1}{2} La_s s_{p1} - \frac{1}{2} Ls_1 s_{p1} + \frac{1}{2} Ls_p s_{p1}\right)\left(2Re_{E1} a_{lpf} a_p + a_{lpf} e_{1star} s_{p1} + s_{p1}^2 e_{1star}\right)\left(a_f + s_{p1}\right)}$$

Fig. 6. Depiction of the MMC TF derivation